



Clusters of vortices induced by thermal gradient in mesoscopic superconductors [☆]



Lucas Veneziani de Toledo ^a, Alice Presotto ^b, Leonardo Rodrigues Cadornim ^a, Daví Filenga ^a, Rafael Zadorosny ^b, Edson Sardella ^{a,*}

^a Departamento de Física, Faculdade de Ciências, Universidade Estadual Paulista (UNESP), Caixa Postal 473, 17033-360, Bauru-SP, Brazil

^b Departamento de Física e Química, Faculdade de Engenharia de Ilha Solteira, Universidade Estadual Paulista (UNESP), Ilha Solteira, Brazil

ARTICLE INFO

Article history:

Received 1 March 2021

Received in revised form 25 April 2021

Accepted 20 May 2021

Available online 26 May 2021

Communicated by L. Ghivelder

Keywords:

Thermal gradient

Time dependent Ginzburg-Landau equations

Giant vortex

Cluster of vortices

Non-monotonic vortex-vortex interaction

ABSTRACT

The structural and magnetic properties of the vortex matter in mesoscopic superconductors have been of great interest in the last decades. Recently, it has been found that vortex-vortex interaction, which is generally repulsive, can be non-monotonic under some special circumstances. Here, we have studied this issue by applying the three dimensional time dependent Ginzburg-Landau equations to a thin type-I mesoscopic superconducting film under a thermal gradient. We find that this favors the formation of small clusters of vortices in some special domains of the superconductor. We also find that this is intimately related to the non-monotonic vortex-vortex interaction by investigating the behavior of two constrained vortices in the presence of a thermal gradient. We show that the vortex-vortex interaction alternates between short range attraction and long range repulsion. This study shows that the thermal gradient has the potential to be an important tool to manipulate the vortex matter.

© 2021 Elsevier B.V. All rights reserved.

1. Introduction

Perhaps one of the most important features of superconductors, both from the viewpoint of their fundamental properties as well as their possible applications, is the behavior of topological excitations in the superconducting state. The most well known and long studied example of such excitations is the magnetic flux line (*i.e.* vortex), at which center the phase of the superconducting order parameter ψ rotates by a multiple of 2π , consequently limiting the amount of flux carried by each vortex in integer multiples of the magnetic flux quanta Φ_0 [1,2].

Vortices were first predicted to exist in the superconducting state within the framework of the Ginzburg-Landau (GL) theory by A. Abrikosov [3], who showed that, for type-II superconductors, vortices are thermodynamically stable above the first critical field H_{c1} . A superconductor is classified as type-II when its GL parameter κ is larger than $1/\sqrt{2}$. Due to the negative surface energy between superconducting and normal regions for type-II superconductors, the flux lines tends to maximize their surface area, thus rendering the vortex-vortex interaction repulsive. On the

other hand, for type-I superconductors ($\kappa < 1/\sqrt{2}$), although isolated vortices are thermodynamically unstable, the surface energy between superconducting and normal regions is positive, which means that the vortex-vortex interaction is attractive and the magnetic flux lines merge into each other to form patterns highly dependent of the sample geometry.

At the special case $\kappa_c = 1/\sqrt{2}$, known as the Bogomolnyi point, it was shown that the two GL equations become self-dual and every vortex configuration has precisely the same energy, *i.e.*, vortices do not interact at κ_c [4]. Nevertheless, even slightly below the critical temperature T_c though, this simple textbook description ceases to be valid at the vicinity of κ_c [5], where non-local effects not present in the standard GL theory become important. In fact, it was shown that, upon extending the standard GL expansion in the parameter $\tau = 1 - T/T_c$ to the next-to-leading order, an intertype domain in the $\kappa - T$ space emerges, in which vortex-vortex interaction are now non-monotonic, namely, short-range repulsive and long-range attractive [6,7].

In addition to the aforementioned non-local effects, it is also known that geometrical effects are also able to break the Bogomolnyi self-duality below T_c , even in the standard GL picture, thus also giving rise to the intertype domain. In particular, it was shown [8–11] that thin-films of type-I superconductors move from a type-I to a type-II behavior, passing by the intertype domain, as the film thickness is decreased. This occurs due to the stray field effects, which contributes to the vortex-vortex interaction with a

[☆] This document is the result of the research project funded by the Brazilian Agency FAPESP-Fundação de Amparo a Pesquisa do Estado de São Paulo, processes numbers 19/24618-0, 20/03947-2, 20/10058-0.

* Corresponding author.

E-mail address: edson.sardella@unesp.br (E. Sardella).

repulsive term. In the thickness region, where the intertype phase exists, the vortex-vortex attraction typical of type-I superconductors competes with the repulsion originated in the stray fields and a non-monotonic interaction results.

In this work, we propose a novel mechanism, based on thermal gradients, to the onset of a non-monotonic vortex-vortex interaction. As in the case of the thin films described above, the non-monotonic interaction reported here does not rely on non-local effects which have already been found in the standard GL formalism. The effects of a thermal gradient on the vortex matter were previously studied [12,13] and shown to develop mainly from a pinning of the vortices in the hotter regions and from an asymmetric penetration of vortices due to the lower penetration field in the sample side with higher temperature.

Here, we show that the presence of a thermal gradient induces the formation of vortex clusters, where vortices tend to agglomerate in specific locations of the sample. Although the sole existence of these vortex clusters indicates that the vortex-vortex interaction is not monotonic, by making use of the constrained GL formalism which fixes the vortex positions [14], we explicitly show that the thermal gradients give rise to a non-monotonic vortex-vortex interaction. The results of the present work are not only of fundamental interest, once it extends previous works on the properties of vortex interactions to systems with a non-homogeneous temperature distributions, but may also be of practical interest, given that this type of thermal gradient could be used to control the vortex matter of superconducting samples [13]. Furthermore, local thermal gradients have already been suggested as a possible route for a series of applications, such as the induction of an open circuit voltage in the absence of an applied current [15] and vortex ratchet effect [16,17].

The outline of this paper is as follows. In Sec. 2 we introduce the theoretical formalism founding our work, which is composed by the time-dependent GL equations (TDGL) and the constrained TDGL equations. In Sec. 3 we present and discuss our main findings, the results of the TDGL equations being reported at Subsec. 3.1 and the those of constrained GL formalism at Subsec. 3.2. Finally, in Sec. 4 we present our final remarks.

2. Theoretical formalism

2.1. TDGL equations

The thermodynamic equilibrium of the superconductors is well described by the Ginzburg-Landau equations (see for instance [1]). Based on first principles, in 1996 Schmid [18] proposed a generalization, commonly known as time dependent Ginzburg-Landau model. They describe the superconductivity in the non-equilibrium state. These equations consider the temporal evolution of the order parameter ψ and of the vector potential \mathbf{A} . In dimensionless units, the TDGL equations are given by

$$\eta \left(\frac{\partial}{\partial t} + i\varphi \right) \psi = -\frac{1}{\kappa^2(0)} (-i\nabla - \mathbf{A})^2 \psi + \frac{\psi}{(1 + \tau^2)^2} (1 - \tau^4 - |\psi|^2), \quad (1)$$

$$\beta \frac{\partial \mathbf{A}}{\partial t} + \nabla \varphi = \mathbf{J}_s - \nabla \times \nabla \times \mathbf{A}, \quad (2)$$

where the superconductivity current density is given by

$$\mathbf{J}_s = \text{Re} \left[\bar{\psi} \left(-\frac{i}{\kappa(0)} \nabla - \mathbf{A} \right) \psi \right]. \quad (3)$$

Here, $\tau = T/T_c$ is the temperature T in units of the critical temperature T_c .

In order to take into account the thermal gradient, we assume that the temperature has a dependency only along the x axis. We have

$$T(x, y, z) = (T_R - T_L)x/l_x + (T_R + T_L)/2, \quad (4)$$

where l_x is the length of the superconductor along the x direction, T_L and T_R are the temperatures on the left and right-hand sides of the superconductor as shown in Fig. 1. It is important to note that our assumption of a linear temperature distribution does not qualitative alter our results if we also assume that the heat removal from the superconductor to the substrate is not strong. This is shown in the Supplementary Material, where we show calculations performed considering the full heat diffusion equation with different heat transfer coefficients.

Once the systems achieves the stationary state, we evaluated the Gibbs free energy through the equation

$$E = -\frac{1}{4} \int_{\Omega_{SC}} \frac{1}{(1 + \tau^2)^2} |\psi|^4 d^3r + \int_{\Omega} (\mathbf{h} - \mathbf{H})^2 d^3r, \quad (5)$$

where Ω_{SC} covers the superconducting domain and Ω the whole space, including the region occupied by the stray fields. Here, \mathbf{H} is the external applied magnetic field.

In order to fulfill the requirement that the critical thermodynamic field relationship, $H_c(\tau) = H_c(0)(1 - \tau^2)$ be valid, we have chosen the phenomenological constants accordingly, so that the coherence and London penetration lengths are given by $\xi(\tau) = \xi(0)\sqrt{(1 - \tau^2)/(1 + \tau^2)}$ and $\lambda(\tau) = \lambda(0)/\sqrt{1 - \tau^4}$, respectively. Within this context, the Ginzburg-Landau parameter is temperature dependent, $\kappa(\tau) = \lambda(\tau)/\xi(\tau) = \kappa(0)/(1 + \tau^2)$ (see References [1], page 106, and [19]).

Due to the temperature dependence of κ , it is important to bear in mind that the results presented below are strictly valid to the average temperature between T_L and T_R used in the calculations. In other words, even if the difference between T_L and T_R is the same, but their average temperature is not, the results would not be the same. As previously shown in Reference [10], this occurs because the crossover between type I and type II superconductivity (and thus from an attraction to a repulsive interaction between vortices) is temperature dependent. Once the intent of the present letter is to show the possibility of a non-monotonic vortex-vortex interaction emerging from a thermal gradient, we do not pursue a more extensive study of the effects of the average temperature on this, which would also require a study with different values of $\kappa(0)$ and different film thicknesses [10].

Dimensionless units were introduced in Eqs. (1)-(3) as follows: the order parameter ψ is in units of $\psi_\infty = \sqrt{\alpha(0)/\beta(0)}$, which is simply the order parameter in the Meissner state at zero temperature, where α and β are two phenomenological constants; length is in units of $\lambda(0)$; magnetic field is in units of $\sqrt{2}H_c(0)$; the vector potential \mathbf{A} is in units of $\sqrt{2}\lambda(0)H_c(0)$; the scalar potential is units of $H_{c2}(0)D/c$, where D is the diffusion coefficient and $H_{c2}(\tau) = \sqrt{2}\kappa(\tau)H_c(\tau)$ is the bulk upper critical field; finally, energy is in units of $E_0 = H_c^2(0)\lambda^3(0)/4\pi$.

Since neither charges nor applied currents are taken into account, we are allowed to use the Coulomb gauge $\varphi = 0$. Thus, it is sufficient to use the following boundary conditions

$$\mathbf{n} \cdot \left(-\frac{i}{\kappa(0)} \nabla - \mathbf{A} \right) = 0, \quad (6)$$

where \mathbf{n} is the unit vector outward normal to the superconductor-vacuum interface, and

$$(\nabla \times \mathbf{A}) \times \mathbf{n} = \mathbf{H} \times \mathbf{n}, \quad (7)$$

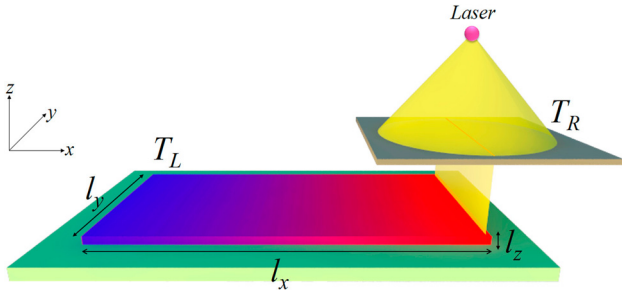


Fig. 1. Sketch of a mesoscopic superconducting stripe. The right-hand side ($x = l_x/2$) end of the sample is heated by a laser at a temperature T_R while the left-hand side end ($x = -l_x/2$) is at the thermal bath temperature $T_L < T_R$. Inside the superconductor, the local temperature varies as $T(x, y, z) = (T_R - T_L)x/l_x + (T_R + T_L)/2$. A mask with a slit is positioned above the superconductor. The radiation produced by the laser passes through the slit with an optical lens which deviates the laser beam straight to the superconducting edge. For sufficiently thin films, the variation of the temperature, from the top to the bottom surface, is very small. Therefore, we can consider its temperature across the thickness film as constant, T_L on the left and T_R on the right-hand side. Notice also that, solely for illustration purposes, we have left a small distance on the right-hand side of laser; this distance is considered so small that the results for the vortex configurations should not be influenced by this approximation.

where \mathbf{n} now represents the unit vector outward normal to the surface of the simulation box. Eq. (6) means $\mathbf{n} \cdot \mathbf{J}_s$ is null at all points on the superconducting surface. On the other hand, Eq. (7) means that the local field is equal to the external applied magnetic field, \mathbf{H} , faraway from the superconductor.

In order to solve Eqs. (1) - (3) numerically, supplied by the boundary conditions (6) and (7) we have used the link-variable method according to References [20–22]. The superconductor of size (l_x, l_y, l_z) is considered inside a simulation box of dimensions (L_x, L_y, L_z) sufficiently large so that the local field becomes uniform on its borders; the simulation box is not shown in Fig. 1, for more details, see figure 1 of Reference [21]. Thus, the boundary condition (7) is fully satisfied. We increase the external applied magnetic field in small steps, typically $\Delta H = 0.001\sqrt{2}H_c(0)$, from zero up to a value for which the superconductor goes to the normal state. During this process, the vortex configuration is arranged in order to minimize the Gibbs free energy so that no restriction is imposed either on ψ or \mathbf{A} . It is in this sense that we will refer to equations ((1)-(3)) *TDGL equations for unconstrained vortices*.

As a final remark, we must emphasize that, although the TDGL equations are most appropriately applied to study the resistive state of superconductors, here we will use them as a relaxation method to obtain the steady state of the vortex state. This is a common practice in the numerical method to solve the standard Ginzburg-Landau equations. We have done this to a mesoscopic superconductor in the presence of thermal gradient which varies linearly from one side of the superconductor to the opposite one. The geometry of the system under investigation is illustrated in Fig. 1.

2.2. TDGL equations for constrained vortices

Now, by *constrained vortices*, such as in [14], we mean two vortices at fixed positions. Let $(l_x/2 - d/2, 0, 0)$ and $(l_x/2 + d/2, 0, 0)$ be the positions of the center of each vortex and d the distance between them. We consider the vortex core center as a straight line along the z direction, so that d is constant. Thus, the order parameter can be written as a superposition of the two vortices

$$\psi(\mathbf{r}) = e^{in_1\theta_1} e^{in_2\theta_2} f(\mathbf{r}), \quad (8)$$

where n_1 and n_2 are the vorticity of both vortices, and

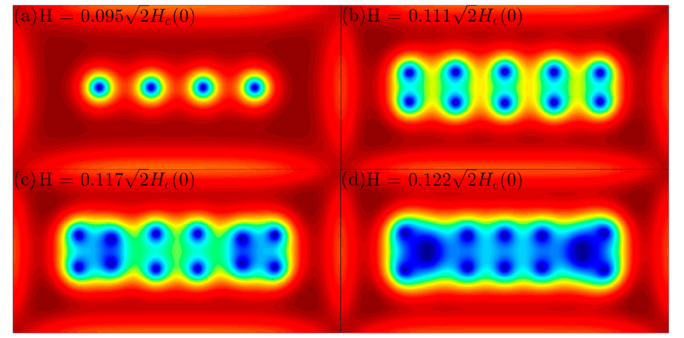


Fig. 2. (Color online.) Intensity of $|\psi|$ for different values of the external magnetic field to $T_L = T_R = 0.75T_c$. The order parameter grows from the dark-blue to the dark-red regions.

$$\theta_k(\mathbf{r}) = \left(\frac{x_k + iy_k}{x_k - iy_k} \right)^{n_k/2}, \quad (9)$$

are the Cartesian form of the phase of each vortex, for $\{k = 1, 2\}$. Here, $\mathbf{r}_1 = (x - l_x/2 - d/2, y, 0)$ and $\mathbf{r}_2 = (x - l_x/2 + d/2, y, 0)$.

Next, by introducing equations (8) and (9) into equations (1) and (2) we obtain

$$\begin{aligned} \frac{\partial f}{\partial t} &= \frac{1}{\kappa^2(0)} \nabla^2 f \\ &\quad - \left[\bar{X}^2 + \bar{Y}^2 + 2(A_x \bar{Y} - A_y \bar{X}) + A^2 \right] f \\ &\quad + \frac{f}{(1 + \tau^2)^2} (1 - \tau^4 - f^2), \end{aligned} \quad (10)$$

$$\frac{\partial \mathbf{A}}{\partial t} = \left[\mathbf{A} - \frac{n_1}{r_1} \hat{\theta}_1 - \frac{n_2}{r_2} \hat{\theta}_2 \right] f^2 - \nabla \times \nabla \times \mathbf{A}, \quad (11)$$

where

$$\bar{X} = \frac{n_1 x_1}{r_1^2} + \frac{n_2 x_2}{r_2^2}, \quad (12)$$

$$\bar{Y} = \frac{n_1 y_1}{r_1^2} + \frac{n_2 y_2}{r_2^2}, \quad (13)$$

$$\hat{\theta}_k = \left(-\frac{y_k}{r_k}, \frac{x_k}{r_k}, 0 \right). \quad (14)$$

In opposition to what has been considered in Reference [14], we will take into account the demagnetization effects by numerically solving the 3D TDGL equations for constrained vortices.

3. Results and discussion

As sketched in Fig. 1, the system studied here possesses the following parameters: $l_x = 90\lambda(0)$, $l_y = 45\lambda(0)$, $l_z = 2\lambda(0)$, $L_x = 120\lambda(0)$, $L_y = 75\lambda(0)$, $L_z = 40\lambda(0)$, $T_R = 0.85T_c$, $T_L = 0.75T_c$ and GL parameter $\kappa(0) = 0.444$. In order to carry out a comparative study with the system under an applied thermal gradient, we have also investigated the same system, but with the homogeneous distribution of temperatures $T = T_R = T_L = 0.75T_c$, and $T = T_R = T_L = 0.85T_c$. In what follows, we present and discuss the results of the original TDGL equations and the constrained GL equations in Subsec. 3.1 and Subsec. 3.2, respectively.

3.1. Vortex configurations

We begin by presenting and discussing the results for the unconstrained vortices within standard GL theory. In order to investigate how the presence of a thermal gradient affects the vortex configuration, we first present the results for a system with constant temperature over its entire volume. This is done for two

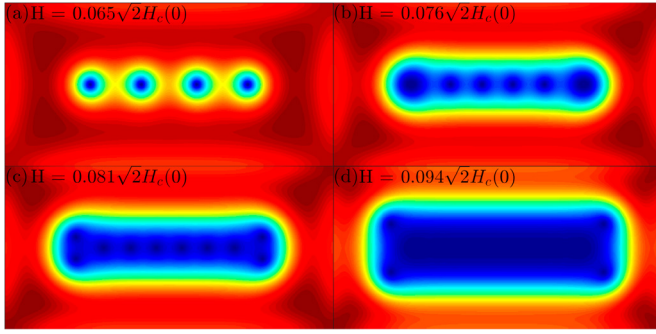


Fig. 3. (Color online.) The same as Fig. 2 for $T_L = T_R = 0.85T_c$.

values of temperature $T = 0.75T_c$ and $T = 0.85T_c$. We then investigate a system whose left side is maintained at a temperature $T_L = 0.75T_c$, while its right side temperature is fixed at $T_R = 0.85T_c$. Fig. 2 shows the color plot of the order parameter for $T_L = T_R = 0.75T_c$ and four different values of the applied field. Panel (a) of Fig. 2 shows the vortex configuration for $H = 0.095\sqrt{2}H_c(0)$. As can be seen, a single row with four vortices is formed along the x direction of the film. This occurs once the vortices repel each other, thus being energetically favorable a configuration with the largest possible inter-vortex distance. Note that, once the GL parameter $\kappa(0) < 1/\sqrt{2}$, the vortex-vortex repulsive interaction occurs due to the stray fields.

For a larger applied field $H = 0.111\sqrt{2}H_c(0)$, shown in panel (b) of Fig. 2, six more vortices penetrate the sample, which now presents two parallel rows with five vortices each. At this field, the vortices can still organize themselves inside the superconductor in a regular pattern without deformation. Nevertheless, as the magnetic field is further increased, the number of vortices becomes larger and confinement effects become more visible, as in the case of panel (c), which presents the color plot for $H = 0.117\sqrt{2}H_c(0)$, where two more vortices penetrate the sample and their arrangement becomes distorted. For $H = 0.122\sqrt{2}H_c(0)$ (panel (d)), as even more vortices are nucleated, this behavior is further enhanced mainly near the edges of the superconductor, where confinement effects caused by the screening currents are stronger.

Now, Fig. 3 shows the color plot for $T_L = T_R = 0.85T_c$, also for four different values of the applied field. For $H = 0.065\sqrt{2}H_c(0)$ (panel (a)), as in the case of panel (a) of Fig. 2, four vortices are displayed in a row inside the superconductor. Due to the higher temperature, the size of the vortex core now is larger, but the vortices are also organized in such a way to achieve maximum inter-vortex distance. However, this larger vortex size enhances the interaction of the vortices with surface currents, thus increasing the confinement effects. This is seen already in panel (b), which shows the color plot for $H = 0.076\sqrt{2}H_c(0)$. As the magnetic field is further increased these confinement effects appear more clearly and the larger vortex size makes the cores of the vortices to overlap, creating a region of suppressed superconductivity in the center of the sample, as can be seen in panels (c) and (d).

Finally, we discuss the vortex configuration in the presence of a thermal gradient, where $T_L = 0.75T_c$ and $T_R = 0.85T_c$ (see Fig. 4). The major difference between this and the previous cases is already evident in panel (a), which shows the color plot of the order parameter for $H = 0.076\sqrt{2}H_c(0)$. Here, as has been discussed previously, the four vortices are displayed in a row, but now the inter-vortex distances vary, being shorter in the hotter region than in the colder one. If the equal and maximum possible separation of the previous cases meant a repulsive vortex-vortex interaction, the distribution now encountered suggests that this interaction can also be attractive in the presence of a thermal gradient. Panel (b), which represents the case of $H = 0.079\sqrt{2}H_c(0)$, gives further evidence for this. As more vortices penetrate the sam-

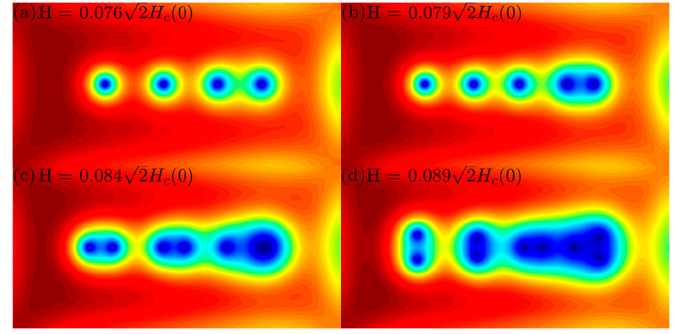


Fig. 4. (Color online.) The same as Fig. 2 for $T_L = 0.75T_c$ and $T_R = 0.85T_c$.

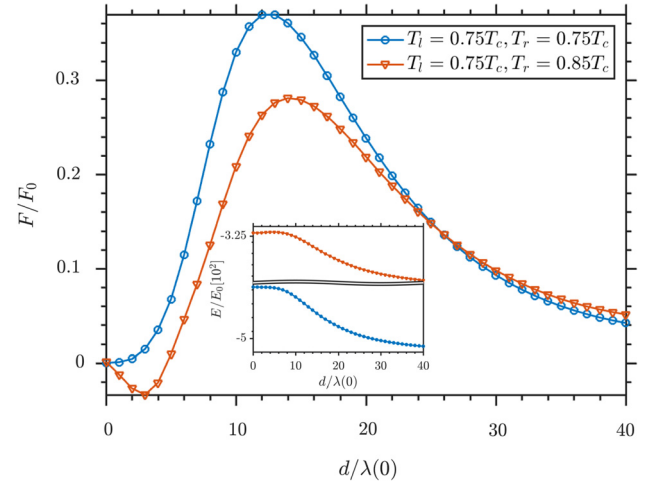


Fig. 5. (Color online.) Force (in units of $F_0 = H_c^2(0)\lambda^2(0)/4\pi$) as a function of the distance between two constrained vortices for homogeneous temperature, and for a thermal gradient as indicated in the legend of the figure. Inset: the energy of the respective configurations.

ple, the formation of vortex clusters gets more visible in the hotter region. For $H = 0.084\sqrt{2}H_c(0)$ (panel (c)) the formation of vortex clusters can be seen also in the colder region and the emergence of a non-monotonic vortex-vortex interaction becomes clearer. For even higher values of the applied field (panel (d)) the vortex cores overlap in the hotter region (where the coherence length is larger) and the visualization of the vortex pattern becomes more difficult. To fully prove the non-monotonicity of the vortex-vortex interaction indicated by the formation of vortex clusters discussed above, one needs to access the energy profile of the vortex configurations and study how it evolves as the inter-vortex distances are changed. Such an analysis is provided in the next section.

3.2. Vortex-vortex interaction

Let us now prove that the presence of a thermal gradient indeed induces a non-monotonic vortex-vortex interaction. To do this, we use the constrained GL formalism to calculate how the energy of a two-vortex configuration changes as we change the distance between them. As done in [14], in order to eliminate boundary effects in the vortex-vortex interaction, the calculations are realized in the absence of an applied field. The general procedure is as follows. We start with two vortices at the center of the superconductor (*i.e.* $(x, y, z) = (l_x/2, l_y/2, l_z/2)$) and then slowly move them apart along the x axis, by taking one towards the left and the another one in the opposite direction, keeping the y coordinate constant. For each vortex-vortex distance d , the energy of the system is then calculated.

The inset of Fig. 5 shows the energy as a function of d for the case without a thermal gradient (blue curve) with $T_L = T_R = 0.75T_c$ and for the case with the presence of a thermal gradient (orange curve) with $T_L = 0.75T_c$ and $T_R = 0.85T_c$. From these curves, the interaction force between the two vortices can be computed. Both cases are displayed in Fig. 5. As we can see from the blue curve, the interaction between the vortices is always repulsive in absence of a thermal gradient. This is in accordance, for example, with panel (a) of Fig. 2, where the vortices organize themselves in such a way as to achieve the greatest possible distance from each other.

On the other hand, the orange curve exhibits a more complex behavior, with the emergence of a distance region where the vortex-vortex interaction is attractive. As we can see, the inter-vortex interaction in this case is only repulsive for a vortex separation $d \gtrsim 6\lambda(0)$, while for small inter-vortex distances ($d \lesssim 6\lambda(0)$) there is an attraction between the vortices. One can then immediately see that the asymmetry between the left and right sides of the sample induced by the thermal gradient causes the emergence of a short range attraction between two vortices being symmetrically displaced from the center of the superconductor.

This confirms that, as suggested by the formation of vortex clusters discussed in the previous section, the thermal gradient induces a non-monotonic vortex-vortex interaction in the direction of the thermal gradient. This occurs due to the fact that, in the presence of a thermal gradient, the system becomes inhomogeneous and the vortices prefer to be in the hotter region of the superconductor. Thus, the non-monotonic vortex-vortex interaction arises as a competition between vortex-vortex repulsion that would exist without the thermal gradient and the tendency of the vortex to be on the hotter region. In the Supplementary Material we show the interaction profile for different thermal gradient intensities, but maintaining the average temperature between T_L and T_R equals to $T = 0.80T_c$. As can be seen from this interaction, the non-monotonic behavior presented here persists for a wide range of gradient intensities.

Now, the above analysis holds only if the two vortices are displaced symmetrically from the center of the superconductor (recall that our sample is inhomogeneous). Thus, to discuss the vortex clusters presented before, we need a more specific investigation. The results are shown in Fig. 6, where we now study the energy for three-vortex configuration. Here, the external field is taken as $H = 0.73\sqrt{2}H_c$ and two vortices (the left and right ones) are fixed at the positions which come out from the unconstrained TDGL simulation for the same value of H . The position of the third vortex in between is then varied and we search for the configuration of minimal energy.

Panel (a) of Fig. 6 shows the energy as a function of the third vortex position and panels (b) – (e) show the color plot of some special configurations. As one can see, as the vortex moves from the position of the left fixed vortex (panel (b)) the configuration energy decreases (panel (c)) until the system reaches its minimum energy value at $x = 3.5\lambda(0)$ (panel (d)). If we now move the vortex closer to right fixed vortex, the energy starts increasing again.

As expected, the configuration with minimum energy (panel (d)) coincides exactly with the configuration encountered from the unconstrained TDGL simulations. This can be seen in the inset of panel (a) of Fig. 6, where we plot the modulus of the order parameter along the central line of the superconducting stripe as a function of the position x . The blue and orange curves correspond to the results for the unconstrained and constrained simulations, respectively. They coincide almost exactly with small deviation around the center of the sample.

Fig. 6(a) also confirms our previous analyses that the thermal gradient makes it energetically favorable for the vortex to be on the hotter region, once the optimal position of the free vortex is

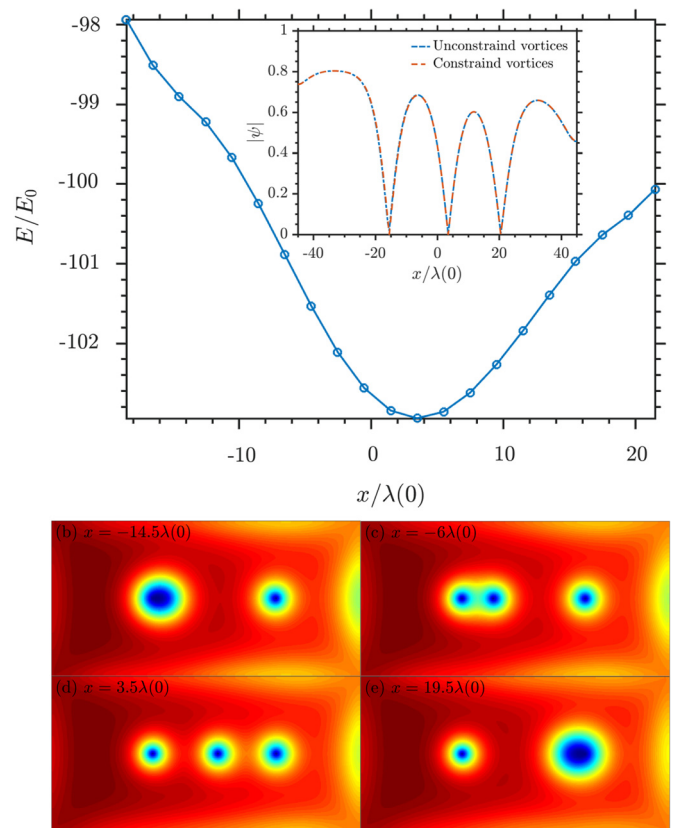


Fig. 6. (Color online.) a) Energy of a three-vortex system with the two ends being fixed and the middle one free to move. The energy is plotted as a function of the position of the middle vortex. The inset shows the order parameter along the line $y = 0$ for both the constrained vortices and those which come out from the conventional TDGL equations of Section 2.2. a) – b) Four distinct configurations of the constrained three-vortex system.

closer to the right fixed vortex rather than to the left one. This can also be seen from the fact that the configuration energy is higher when the free vortex is closer to the left fixed vortex, reflecting once more the “attraction” exercised by the hotter region.

4. Concluding remarks

In summary, we have shown that the application of a thermal gradient in a superconducting film favors the formation of vortex clusters. These clusters result from the competition between the inter-vortex repulsion due to the stray fields and the tendency of the vortex to occupy the hotter region of the sample. Indeed, as shown by the analysis of the constrained Ginzburg-Landau equations, this competition results in the emergence of a non-monotonic vortex-vortex interaction, which does not only depend on the inter-vortex distances, as in films with uniform temperature distribution, but also on the position of the vortex relative to the thermal gradient. This is to be expected, once the hotter region exerts the effect of a pinning center. The present preliminary investigation suggests that thermal gradients can be used to manipulate the vortex matter configurations, in particular to create a non-uniform vortex distribution.

CRediT authorship contribution statement

Lucas Veneziani de Toledo: Conducted the simulations, contributed to the illustration of the figures. **Alice Presotto:** Contributed to the discussion of the results. **Leonardo Rodrigues Cadornim:** Conducted the simulations, wrote the manuscript. **Davi Filenga:** Contributed to the illustration of the figures, contributed

to the discussion of the results. **Rafael Zadorosny**: Contributed to the conceptualization of the problem. **Edson Sardella**: Contributed to the conceptualization of the problem, revised the manuscript, supervised the work.

Declaration of competing interest

The authors declare that they have no known competing financial interests or personal relationships that could have appeared to influence the work reported in this paper.

Appendix A. Supplementary material

Supplementary material related to this article can be found online at <https://doi.org/10.1016/j.physleta.2021.127449>.

References

- [1] M. Tinkham, Introduction to Superconductivity, 2nd edition, Dover Publications, 2004, <https://store.doverpublications.com/0486435032.html>.
- [2] P.-G. De Gennes, Superconductivity of Metals and Alloys, CRC Press, 2018, <https://www.routledge.com/Superconductivity-Of-Metals-And-Alloys/Gennes/p/book/9780738201016>.
- [3] A.A. Abrikosov, On the magnetic properties of superconductors of the second group, Sov. Phys. JETP 5 (1957) 1174–1182, Zh. Eksp. Teor. Fiz. 32 (1957) 1442, http://www.jetp.ac.ru/cgi-bin/dn/e_005_06_1174.pdf.
- [4] E.B. Bogomolny, The stability of classical solutions, Sov. J. Nucl. Phys. 24 (1976) 449–454, <https://www.doccity.com/pt/the-stability-of-classical-solutions/4895287/>.
- [5] I. Luk'yanchuk, Theory of superconductors with κ close to $1/\sqrt{2}$, Phys. Rev. B 63 (2001) 174504, <https://doi.org/10.1103/PhysRevB.63.174504>.
- [6] A.V. Vagov, A.A. Shanenko, M.V. Milošević, V.M. Axt, F.M. Peeters, Extended Ginzburg–Landau formalism: systematic expansion in small deviation from the critical temperature, Phys. Rev. B 85 (2012) 014502, <https://doi.org/10.1103/PhysRevB.85.014502>.
- [7] A. Vagov, A.A. Shanenko, M. Milošević, V.M. Axt, V.M. Vinokur, J.A. Aguiar, F.M. Peeters, Superconductivity between standard types: multiband versus single-band materials, Phys. Rev. B 93 (2016) 174503, <https://doi.org/10.1103/PhysRevB.93.174503>.
- [8] W.Y. Córdoba-Camacho, R.M. da Silva, A. Vagov, A.A. Shanenko, J.A. Aguiar, Between types I and II: intertype flux exotic states in thin superconductors, Phys. Rev. B 94 (2016) 054511, <https://doi.org/10.1103/PhysRevB.94.054511>.
- [9] W.Y. Córdoba-Camacho, R.M. da Silva, A. Vagov, A.A. Shanenko, J.A. Aguiar, Quasi-one-dimensional vortex matter in superconducting nanowires, Phys. Rev. B 98 (2018) 174511, <https://doi.org/10.1103/PhysRevB.98.174511>.
- [10] L.R. Cadorim, T. de Oliveira Calsolari, R. Zadorosny, E. Sardella, Crossover from type I to type II regime of mesoscopic superconductors of the first group, J. Phys. Condens. Matter 32 (9) (2019) 095304, <https://doi.org/10.1088/1361-648x/ab4a4a>.
- [11] W.Y. Córdoba-Camacho, R.M. da Silva, A.A. Shanenko, A. Vagov, A.S. Vasenko, B.G. Lvov, J.A. Aguiar, Spontaneous pattern formation in superconducting films, J. Phys. Condens. Matter 32 (7) (2019) 075403, <https://doi.org/10.1088/1361-648x/ab5379>.
- [12] E.C.S. Duarte, A. Presotto, D. Okimoto, E. Sardella, R. Zadorosny, Influence of thermal gradient in vortex states of mesoscopic superconductors, J. Phys. Conf. Ser. 568 (2) (2014) 022011, <https://doi.org/10.1088/1742-6596/568/2/022011>.
- [13] E.C.S. Duarte, A. Presotto, D. Okimoto, V.S. Souto, E. Sardella, R. Zadorosny, Use of thermal gradients for control of vortex matter in mesoscopic superconductors, J. Phys. Condens. Matter 31 (40) (2019) 405901, <https://doi.org/10.1088/1361-648x/ab2d70>.
- [14] A. Chaves, F.M. Peeters, G.A. Farias, M.V. Milošević, Vortex-vortex interaction in bulk superconductors: Ginzburg–Landau theory, Phys. Rev. B 83 (2011) 054516, <https://doi.org/10.1103/PhysRevB.83.054516>.
- [15] C. Xue, A. He, M.V. Milošević, A.V. Silhanek, Y.-H. Zhou, Open circuit voltage generated by dragging superconducting vortices with a dynamic pinning potential, New J. Phys. 21 (11) (2019) 113044.
- [16] A. He, C. Xue, Y.-H. Zhou, Switchable reversal of vortex ratchet with dynamic pinning landscape, Appl. Phys. Lett. 115 (3) (2019) 032602.
- [17] A. He, C. Xue, Multiple reversals of vortex ratchet effects in a superconducting strip with inclined dynamic pinning landscape, Chin. Phys. B 29 (12) (2020) 127401.
- [18] A. Schmid, A time dependent Ginzburg–Landau equation and its application to the problem of resistivity in the mixed state, Phys. Kondens. Mater. 5 (4) (1966) 302–317.
- [19] V.I. Ginzburg, Some remarks concerning the macroscopic theory of superconductivity, Sov. Phys. JETP 3 (4) (1956) 621.
- [20] W.D. Gropp, H.G. Kaper, G.K. Leaf, D.M. Levine, M. Palumbo, V.M. Vinokur, Numerical simulation of vortex dynamics in type-II superconductors, J. Comput. Phys. 123 (2) (1996) 254–266, <https://doi.org/10.1006/jcph.1996.0022>, <http://www.sciencedirect.com/science/article/pii/S0021999196900224>.
- [21] J. Barba-Ortega, E. Sardella, J.A. Aguiar, Superconducting properties of a parallelepiped mesoscopic superconductor: a comparative study between the 2D and 3D Ginzburg–Landau models, Phys. Lett. A 379 (7) (2015) 732–737, <https://doi.org/10.1016/j.physleta.2014.12.030>, <http://www.sciencedirect.com/science/article/pii/S0375960114012705>.
- [22] J. Barba-Ortega, E. Sardella, Superconducting properties of a mesoscopic parallelepiped with anisotropic surface conditions, Phys. Lett. A 379 (47) (2015) 3130–3135, <https://doi.org/10.1016/j.physleta.2015.10.013>, <http://www.sciencedirect.com/science/article/pii/S0375960115008701>.